Hindawi
Advances in Materials Science and Engineering
Volume 2021, Article ID 6651633, 10 pages
https://doi.org/10.1155/2021/6651633

Research Article

In Situ g-C_3N_4@Zno Nanocomposite: One-Pot Hydrothermal Synthesis and Photocatalytic Performance under Visible Light Irradiation

Lan Anh Luu Thi,[1] **Mateus Manuel Neto**,[2] **Thang Pham Van**,[1] **Trung Nguyen Ngoc**,[1] **Tuyet Mai Nguyen Thi**,[3] **Xuan Sang Nguyen**,[4] **and Cong Tu Nguyen**[1]

[1]*School of Engineering Physics, Hanoi University of Science and Technology, Hanoi, Vietnam*
[2]*Agostinho Neto University, University City District, Stadium 11 November Street, Campus University Agostinho Neto, Luanda, Angola*
[3]*School of Chemical Engineering, Hanoi University of Science and Technology, Hanoi, Vietnam*
[4]*Department of Electronics and Telecommunication, Saigon University, 273 An Duong Vuong, Ward 3, District 5, Ho Chi Minh city 084-08, Vietnam*

Correspondence should be addressed to Lan Anh Luu Thi; anh.luuthilan@hust.edu.vn

Received 4 December 2020; Accepted 3 May 2021; Published 11 May 2021

Academic Editor: Matjaz Valant

In situ g-C_3N_4@ZnO nanocomposites (with 0, 1, 3, 5, and 7 wt.% of g-C_3N_4 in nanocomposite) were synthesized via a one-pot hydrothermal method using precursors of urea, zinc nitrate hexahydrate, and hexamethylenetetramine. The g-C_3N_4@ZnO nanocomposites were characterized by X-ray diffraction, scanning electron microscope, diffuse reflectance spectroscopy, and photoluminescence spectroscopy. The photocatalyst activity of g-C_3N_4@ZnO nanocomposites was evaluated via methylene blue degradation experiment under visible light irradiation. The g-C_3N_4@ZnO nanocomposites showed an enhancement in photocatalytic activity in comparison to pure ZnO which increased with the g-C_3N_4 content (1, 3, 5, and 7 wt.%) in nanocomposites. The photocatalytic activity reached the highest efficiency of 96.8% when the content of g-C_3N_4 was 7.0 wt.%. Nanocomposite having 7.0 wt.% of g-C_3N_4 also showed good recyclability with degradation efficiency higher than 90% even in the 4th use. The improvement of photocatalytic activity could be attributed to the adsorption ability and effective separation of electron-hole pairs between g-C_3N_4 and ZnO. This work implies a simple method to in situ prepare the nanocomposite material of g-C_3N_4 and semiconductors oxide for photocatalyst applications with high efficiency and good recyclability.

1. Introduction

The economic development in recent decades has led to very serious environmental problems due to the uncontrolled release of harmful pollutants in water and air. Developing cost-effective and simple technologies for removing harmful pollutant is one of the most attentive matters to research recently [1–3]. Photocatalysis is considered a promising technique to treat contaminated water because the photocatalysis process is eco-friendly and economical and is capable of degrading several organic dyes or pollutants [1, 4–13].

Zinc oxide (ZnO) is a metal oxide semiconductor with a direct wide bandgap (3.2 eV), high mechanical, thermal, and chemical stability, nontoxic nature, and low cost [14–16]. ZnO is considered one of the most promising materials for photocatalytic application. However, due to the large bandgap, ZnO exhibits relatively low photocatalytic activity under visible light in comparison with under UV light. Moreover, the fast recombination of charge carriers in ZnO restricts its practical applicability [15, 17–20]. To efficiently overcome these limitations, many efforts shave been made to improve the photocatalytic activity of ZnO-based

photocatalysts through doping or compositing with metals, nonmetals, carbon-based materials (graphene, graphene oxide, and reduced graphene oxide) [21, 22] or coupling with visible bandgap semiconductor to create Z-scheme [15, 23, 24]. However, the development of an efficient ZnO-based photocatalyst with improved photocatalytic efficiency is still in progress.

Graphitic carbon nitride (g-C_3N_4) is a stable, metal-free, *p*-conjugative, and n-type polymeric semiconductor with a narrow bandgap (2.7 eV) [23] which could act as a desirable partner to ZnO to make a good visible-light-responsive photocatalytic composite [25–28]. Therefore, coupling ZnO with g-C_3N_4 could yield an excellent heterostructure to improve charge separation, especially since the two materials have well-matched, overlapping band structures. Previous research has shown that these heterostructures exhibit an improvement in photocatalytic activity. The improvement is explained via the transfer of a visible-light-induced electron from the conduction band (CB) of the g-C_3N_4 to the CB of ZnO [2, 29–31].

In this paper, an attempt has been made to prepare and characterize in situ nanocomposite g-C_3N_4@ZnO using the one-pot hydrothermal method at low temperature. Effects of g-C_3N_4 content on the microstructural, optical properties and photocatalytic activities of g-C_3N_4@ZnO were investigated via X-ray diffraction, PL spectra, diffuse reflectance spectra, and scanning electron microscopy analysis. The photocatalytic activity was evaluated through the degradation experiment of methylene blue (MB) dye under visible-light irradiation. The recyclability of nanocomposite was also studied. Besides, the photocatalytic mechanism of g-C_3N_4@ZnO was also discussed.

2. Materials and Methods

2.1. Samples Preparation. All chemicals were of analytical grade and were used without any further purification. Graphitic carbon nitride (g-C_3N_4) was synthesized by pyrolyzing urea in a muffle furnace at 520°C for 2h. After cooling down gradually to room temperature (RT), the annealed sample was ground by an agate mortar to obtain the g-C_3N_4 powder in light yellow colour for further use.

Nanocomposites of zinc oxide and graphitic carbon nitride were synthesized by the one-step hydrothermal method via the following process: dissolving 1.485 g $Zn(NO_3)_2.6H_2O$ into 50 ml bidistilled water, dissolving 0.700 g HMTA into 50 mL bidistilled water, mixing two solutions with the [HMTA]/[Zn^{2+}] volume ratio of 1 : 1 under stirring for 10 mins at RT, and adding g-C_3N_4 into these solutions. The resulting mixture was transferred to an autoclave for the hydrothermal route at 90°C for 6 h. The products were collected and rinsed twice with absolute ethanol and distilled water and then dried in the oven at 80°C for 24 h. Finally, a fine white to grey powder was obtained. We named the samples prepared with different g-C_3N_4 content as 1, 3, 5, and 7 wt.% as Z-1C, Z-3C, Z-5C, and Z-7C, respectively.

2.2. Characterization. The crystal structure and phase purity were obtained by using the X-ray diffraction (XRD) system of X'Pert Pro (PANalytical) MPD with CuK-α1 radiation (= 1.54056 Å) at a scanning rate of 0.03°/2s in the 2θ range from 20° to 80°. The crystal analysis was performed by HighScore Plus software using the ICDD database. The morphology of the g-C_3N_4@ZnO nanocomposite was analysed by scanning electron microscopy (SEM). The distribution of g-C_3N_4 in the ZnO platform was evaluated via the elemental mapping images using Tabletop Microscope HITACHI TM4000Plus. The diffusion reflectance spectra of samples were obtained by JASCO V-750 using 60 mm Integrating Sphere ISV-922. The PL spectra of the samples were measured by NanoLog fluorescence spectrometer (HORIBA JOBIN YVON) with imaging spectrometer iHR 320 and xenon lamp light source with an excitation wavelength of 325 nm.

2.3. Photocatalytic Experiment. The photocatalytic efficiencies of the g-C_3N_4@ZnO nanocomposites and pristine ZnO were evaluated via methylene blue (MB) degradation experiment at room temperature. Typically, 50 mg of the photocatalyst was dispersed in 100 mL MB aqueous solution (10 mg/L). The above mixture was stirred in dark for 60 min to achieve an adsorption-desorption equilibrium. The mixture was then illuminated under visible irradiation using a 250 W Osram lamp equipped with a 420 nm cut-off filter at room temperature. A mixture of 5 mL solution was sampled at each 15-minute interval and then was centrifuged to remove the photocatalyst solids at 7000 rpm for 10 mins. The UV-Vis absorption spectra of the resulting supernatant were measured by a Cary 100 spectrophotometer (VARIAN) to determine the MB concentration.

The degree of MB degradation (D) was estimated through the remaining MB concentration in aliquot which is proportional to the intensity of 664 nm characteristic peak in UV-Vis spectra. The MB degradation is calculated via the following equation:

$$D = \frac{C_o - C_t}{C_o} \times 100\% = \frac{I_o - I_t}{I_o} \times 100\%, \quad (1)$$

where C_o (mg/L) is the initial MB concentration; C_t (mg/L) is the MB concentration in aliquots at time t during the photocatalytic reaction; I_o is the intensity of 664 nm peak in UV-Vis spectrum of initial MB solution. It is the intensity of 664 nm peak in UV-Vis spectrum of aliquots at time t during the photocatalytic reaction.

3. Results and Discussion

3.1. XRD Analysis. The XRD patterns of the g-C_3N_4@ ZnO nanocomposite with g-C_3N_4 contents and ZnO are presented in Figure 1 (the XRD pattern of pure g-C_3N_4; see supplementary figure S1 in which the characteristic peaks of g-C_3N_4 are well observed [31]). The characteristic diffraction peaks of ZnO can be attributed to the hexagonal wurtzite structure (JCPDS 36-1451 card) [32]. The diffraction peaks of a g-C_3N_4@ZnO nanocomposite are similar to those of pure ZnO. No diffraction peaks corresponding to g-C_3N_4 are observed in g-C_3N_4@ZnO nanocomposite. Furthermore, no

other new crystal phases in the preparation process are found.

To understand the effect of g-C_3N_4 on the structure and crystallite size of ZnO, the Williamson-Hall formula is used to analyse the XRD data which is expressed as follows [33–35]:

$$\beta * \cos\theta = \frac{0.9 * \lambda}{D} + 2\varepsilon * \sin\theta, \quad (2)$$

where β is the full width at half maximum of the peak at the diffraction angle 2θ, θ is the diffraction angle, $\lambda = 1.54060$ Å is a wavelength of the used X-ray, ε is the micro strain, and d is the average crystallite size.

A plot of $\beta*\cos\theta$ versus $\sin\theta$ is a linear presentation of the data XRD, and the crystallite size and micro strain are, respectively, obtained from the intercept and slope of the line. The results obtained are listed in Table 1. The results demonstrate that the crystallite size of ZnO is also strongly affected by the appearance of g-C_3N_4, in which the average crystallite size of ZnO reduces from 49.5 nm to 40.8 nm in correspondence with the increase of g-C_3N_4 content in nanocomposite materials. The appearance of g-C_3N_4 also causes the micro strain to reduce in samples where the strain reduces from 0.00407 to 0.00323 when g-C_3N_4 content increases from 1 to 7%. The results show the strong effect of g-C_3N_4 on the crystal properties of in situ nanocomposites.

3.2. SEM Analysis. The SEM observations presented in Figure 2 detail the surface morphologies of the prepared samples. As shown in Figure 2(a), pure g-C_3N_4 is fluffy and porous. Pure ZnO is composed of a large number of aggregated nanorods (Figure 2(b)). Notably, the ZnO nanorods in g-C_3N_4@ZnO nanocomposite are well dispersed over the composite surface (Figures 2(c)–2(f)).

Figure 3 shows the element mapping images including C, N, O, and Zn in g-C_3N_4@ZnO sample with 7 wt.% g-C_3N_4. The mapping images show that the elements C, N, O, and Zn appear in Z-7C and the elements are uniformly distributed in the nanocomposite which also implies that there is coappearance of g-C_3N_4 and ZnO in the nanocomposite.

3.3. UV-Vis Diffuse Reflectance Spectroscopy Analysis. UV-vis diffuse reflectance spectroscopy (DRS) was conducted to investigate the effect of g-C_3N_4 on the optical properties of g-C_3N_4@ZnO samples. The incorporation of g-C_3N_4 into ZnO leads to a decrease in the UV-vis reflectance (or the increase of the absorption) over the entire wavelength range. As presented in Figure 4, the sharp fundamental reflectance edge rises at about 390 nm for the pure ZnO nanorods, with almost no absorption in the visible-light region which is consistent with the fact that ZnO NRs almost can only make use of ultraviolet light [35]. Compared to the pure ZnO and g-C_3N_4, the g-C_3N_4@ZnO extends the absorbance to not only the ultraviolet region but also the visible region, suggesting that the recombination rate of the photoinduced electrohole pairs was successfully reduced in the heterostructured g-C_3N_4@ ZnO nanocomposite.

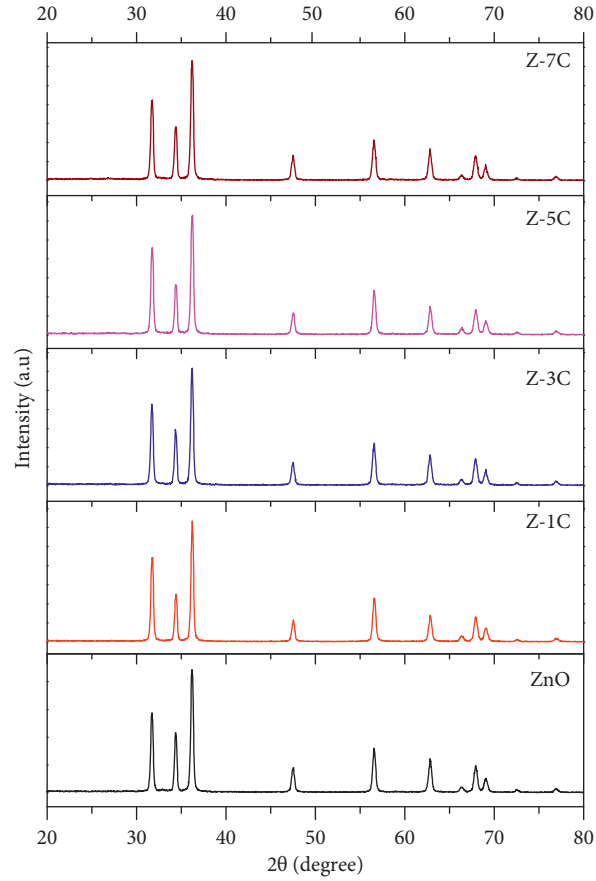

Figure 1: XRD pattern of g-C_3N_4@ZnO nanocomposite samples on the range from 20 to 80°.

Table 1: The average crystallite size of ZnO and nanocomposite samples calculated via Williamson-Hall formula.

Samples	D Williamson-Hall (nm)	Micro strain (ε)	R^2
ZnO	49.5	0.00362	0.9952
Z-1C	47.8	0.00407	0.9921
Z-3C	46.2	0.00392	0.9959
Z-5C	44.7	0.00371	0.9935
Z-7C	40.8	0.00323	0.9931

From the DRS data, there are routes to get the information of bandgap value (called optical bandgap) indirectly using modified Kubelka-Munk function [36–38].

In the Kubelka-Munk method, the relation between the function of diffuse reflectance $F(R)$ and the incident photon energy hν is expressed in the following equation:

$$F(R)h\nu = D\left(h\nu - E_g\right)^n, \quad (3)$$

where $F(R)$ is determined from diffuse reflectance R via the formula $F(R) = (1\text{-}R)^2/2R$; $h\nu$ is the incident photon energy; D is an arbitrary coefficient; $n = ½$ and 2 for direct and indirect allowed recombinations, respectively, and E_g is the optical bandgap of the sample [38].

From this relation, we can extrapolate the value of E_g from the plots of $[F(R)* h\nu]^2$ versus $h\nu$ as shown in Figure 4(b) for ZnO or we can evaluate based on the plot of

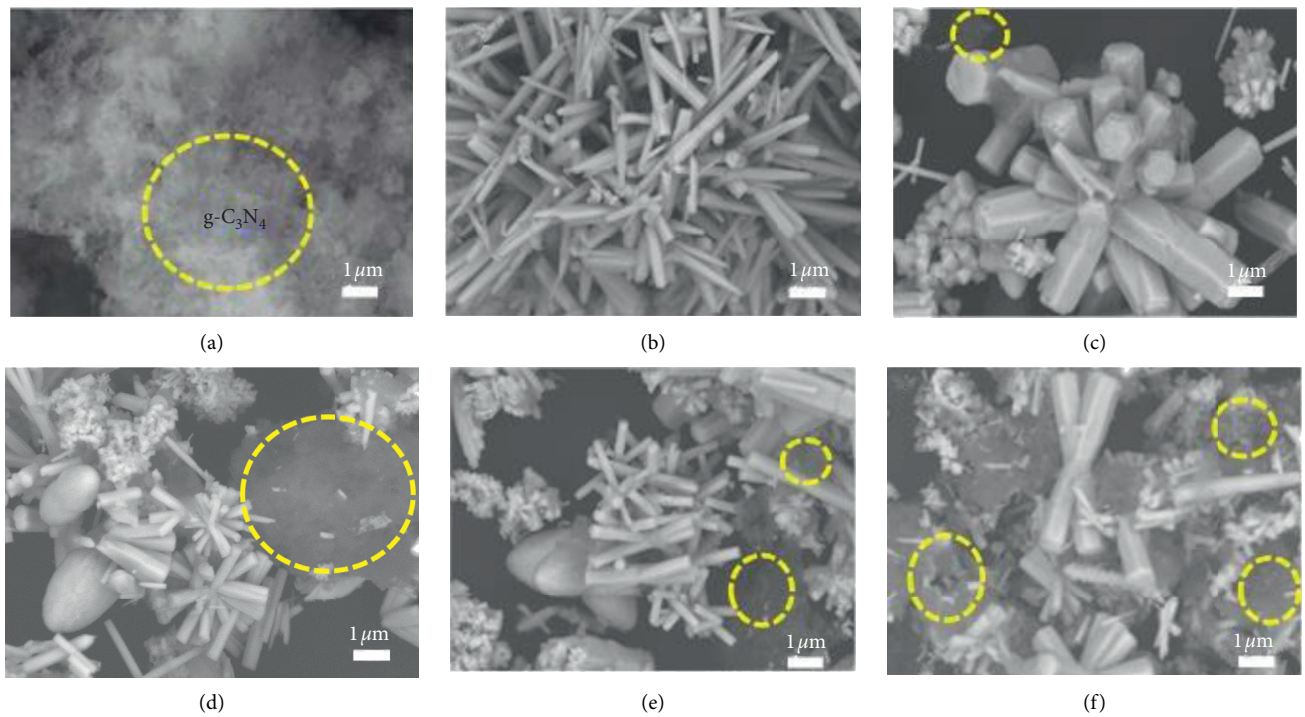

Figure 2: SEM images of (a) g-C_3N_4, (b) ZnO, (c) Z-1C, (d) Z-3C, (e) Z-5C, and (f) Z-7C.

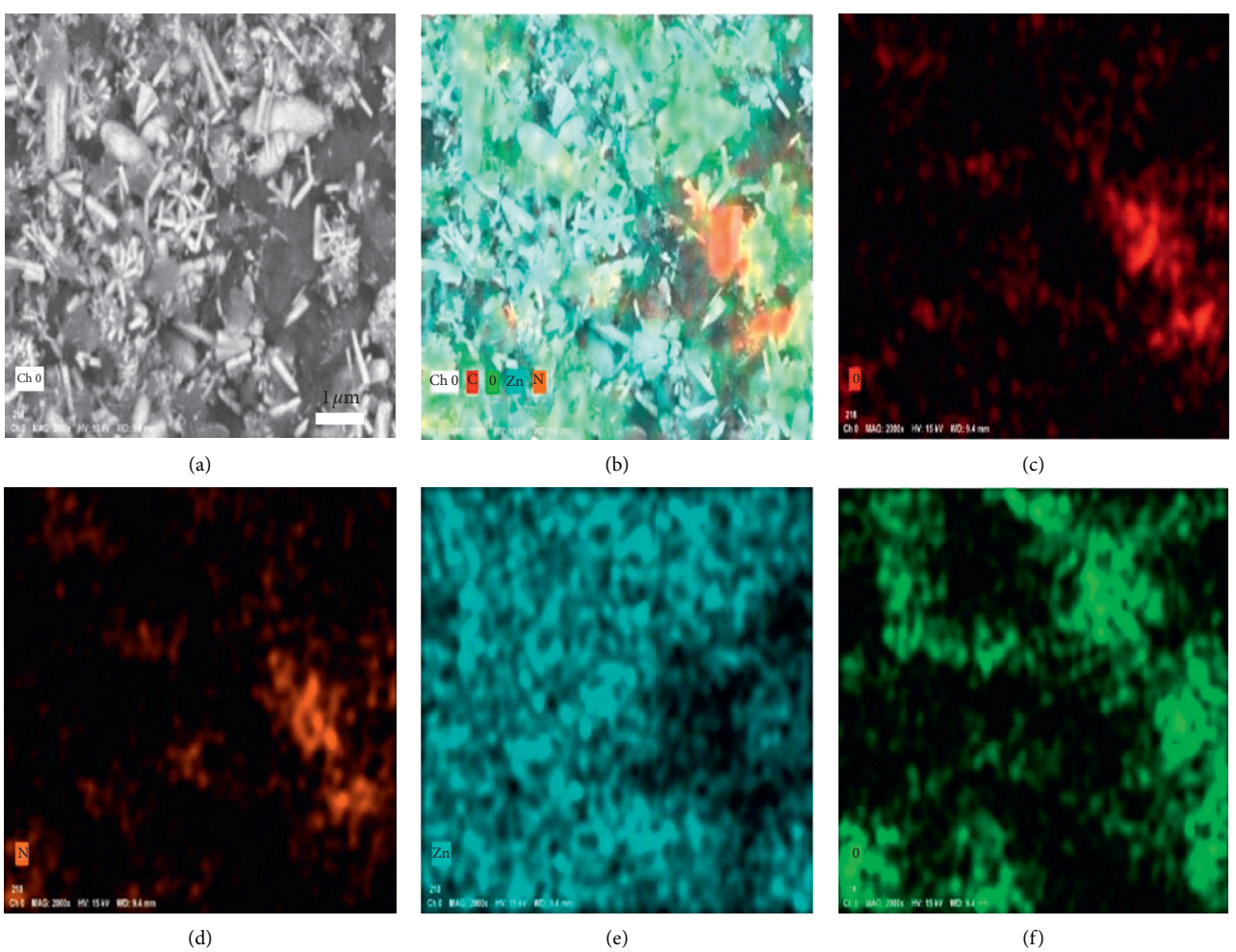

Figure 3: The EDX elemental mapping images of C, N, O, and Zn of Z-7C sample.

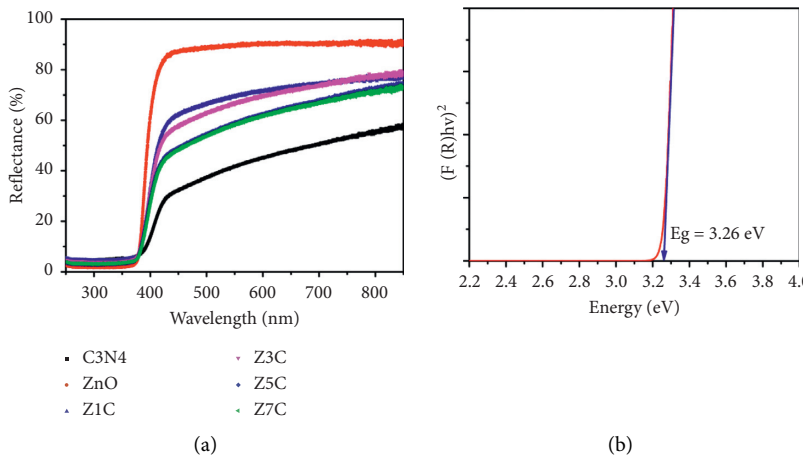

Figure 4: Reflectance spectra of g-C_3N_4@ZnO nanocomposites (a) and $(F\ (R)\ h\nu)^2$ *versus* $(h\nu)$ plot of pure ZnO (b).

$[F(R) * h\nu]^{1/2}$ versus $h\nu$ as shown in Figure S2 for g-C_3N_4 and g-C_3N_4@ZnO. The optical bandgap of the pure g-C_3N_4 has an optical bandgap of 2.85 eV, which agrees well with the previous reports [29, 39, 40]. The pure ZnO nanorod has an optical bandgap of 3.26 eV. Interestingly, the optical bandgap of composites ranges from 3.05 to 3.09 eV and decreases with the increase of g-C_3N_4 content. In detail, the extracted optical bandgaps of nanocomposites Z-1C, Z-3C, Z-5C, and Z-7C are 3.09 eV, 3.08 eV, 3.07 eV, and 3.05 eV, respectively. The decrease in optical bandgap energy results in higher absorption and a higher possibility of photogeneration carriers under visible irradiation. In g-C_3N_4@ZnO composites, the inbuilt electric field on the interface of heterojunction can efficiently promote photocarriers to move to the oriented direction and to change Fermi level. Thus, light absorption and the separation possibility of the photocarriers is enhanced and its photocatalytic performance is further enhanced.

3.4. Photocatalytic Activities. Figure 5(a) presents the absorption spectra of the MB solution mixed with Z-7C samples at different reaction times. It can be seen that Z-7C sample is the absorption peak that reduces continuously with the irradiation time, indicating that the MB aqueous solution is decomposed with the presence of the Z-7C sample under a quasi-sunlight source. To quantify the photocatalytic performance of the synthesized samples in the degradation reaction of the MB, the residual concentration of MB is calculated from the residual intensity of the absorption peak at 664 nm.

Figure 5(b) shows the ratio between the residual MB concentration and the initial MB concentration at different reaction times under visible light using different photocatalytic-blank, pure ZnO, g-C_3N_4, and Z-1C, Z-3C, Z-5C, and Z-7C samples, respectively. All composite samples show good photocatalytic activity under the quasi-sunlight. The photocatalytic performances of blank, pure ZnO, g-C_3N_4, and Z-1C, Z-3C, Z-5C, and Z-7C samples are 4.4%, 24.4%, 82.2%, 65.8%, 92.3%, 93.0%, and 96.8%, respectively. This result implies that the hybridization helps increase the MB degradation under the light irradiation and sample Z-7C shows the highest photocatalytic efficiency. The enhanced photocatalytic activity possibly profited from the efficient photoinduced charge from ZnO to g-C_3N_4.

The MB degradation process was further investigated by the reaction kinetics [39, 41]. The process was fitted via the following equation:

$$\ln\left(\frac{C_0}{C}\right) = kt, \tag{4}$$

where k (min^{-1}) corresponds to the constant rate, C_0 and C represent the MB concentration, and t denotes the reaction time. Figure 5(c) shows the related kinetics data over the catalysts under visible-light irradiation. It can be seen that the regression curve of the natural logarithm of normalized MB concentration versus reaction time is approximately linear, indicating that the kinetics of MB degradation over the photocatalysts follow first-order reaction kinetics.

The fitted constant rate (k) values are presented in Figure 5(d). The degradation rate of the Z-7C nanocomposite was 0.0320 min^{-1}, which is about 24.6 times higher than that of pure ZnO (0.0013 min^{-1}). This indicates that the incorporation of g-C_3N_4on ZnO nanorods has largely influenced the constant rate.

Photocatalytic degradation of MB under visible-light irradiation of Z-7C sample on photocatalytic amount is illustrated in Figure 6(a). It shows an increase in degradation efficiency with the photocatalytic amount. The photocatalytic performance is the highest at 50 mg photocatalyst (Figure 6(b)). However, with the g-C_3N_4@ZnO weight increase exceeding 50 mg, the photocatalytic activities begin to decrease. It is deduced that excess adsorption of MB leads to a decrease in the capacity of light trapping and blocks the generation of photogenerated electrons and holes. The adsorption should achieve suitable intensity, which could guarantee enough photocatalytic activity. Therefore the photocatalyst had realized an optimal balance between MB adsorbing capacity and photon acquisition capability when the weight of g-C_3N_4 was 50 mg.

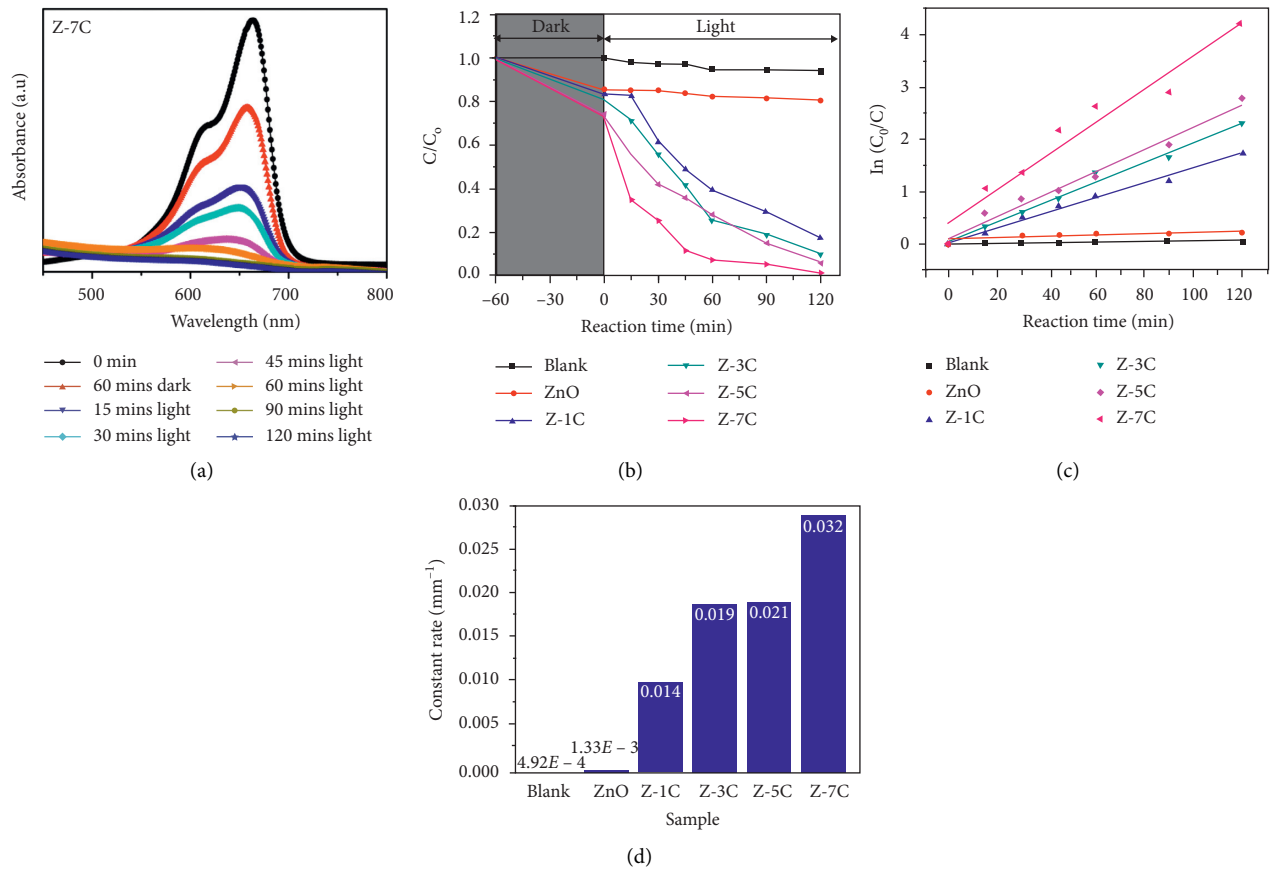

FIGURE 5: (a) Absorption spectra of Z-7C samples. (b) Photocatalytic degradation of MB under visible-light irradiation. (c) Determination of the constant rate (k) of the photocatalytic degradation of MB by kinetic linear simulation plots. (d) The constant rate (k) of the photocatalytic degradation of MB by samples.

Besides, the recyclability of the fabricated g-C_3N_4@ZnO photocatalysts was also studied with 50 mg photocatalyst assessed, and results are shown in Figure 6(c). The recycling experiments were carried out by centrifuging and drying the photocatalyst after the degradation cycle and reusing it during the next cycle. The photocatalytic activity measured under visible-light irradiation, for four cycles, is presented in Figure 6(c). The results demonstrate that the g-C_3N_4@ZnO nanocomposites had stable cyclic performance as a photocatalyst.

The photocatalytic activity of g-C_3N_4@ZnO (7 wt.%) was compared with the previously reported (Table 2). g-C3N4@ZnO is more advantageous than the other catalysts in terms of photocatalytic ability, ease of synthesis, structural stability, and morphologies. Notably, the results presented in Table 2 could not be comparable due to the variation in other experimental conditions such as catalyst amount, power of the light source, distance from the light source, and preparation methodology. The present work possesses the advantage of in situ synthesis of g-C_3N_4@ZnO nanocomposite with enhanced photocatalytic activity.

The steady-state PL spectra were also utilized to examine the separation and recombination processes of the photo-induced electron-hole pairs. A high fluorescence intensity generally corresponds to the significant recombination of electron-hole pairs. Figure 7(a) exhibits the room temperature PL spectra of g-C_3N_4, ZnO, and 7 wt.% g-C_3N_4@ZnO composite samples. As depicted in Figure 7(a), all samples presented a broad luminescence peak, which centres at approximately 450 nm with a certain shift in the peak position with g-C_3N_4 contents. This emission peak is originated from direct band-to-band transitions. This emission peak is originated from direct band-to-band transitions [45–47]. The pure ZnO exhibited a broad intense deep-level (DL) emission which appeared in the range of 400–750 nm [48, 49]. When the g-C_3N_4 ratio increases, the luminescence peak intensity of g-C_3N_4@ZnO composites increases first and then decreases, indicating a more efficient charge carrier pathway formed with a relatively high g-C_3N_4 content. It is also observed that the PL intensity of Z-7C (7 wt.% g-C_3N_4) samples decreased the most in comparison with the bare g-C_3N_4. This result indicates that the g-C_3N_4 @ZnO composite had lower recombination rates of electrons and holes under visible-light irradiation compared to other composites and pristine ZnO and g-C_3N_4.

To probe the active species in the photocatalytic reaction, triethanolamine (TEOA), isopropanol (IPA), and p-benzoquinone (BQ) were introduced into the system as the scavengers of holes (h^+), hydroxyl radicals (·OH), and superoxide radicals ($\cdot O_2^-$), respectively. The measurements

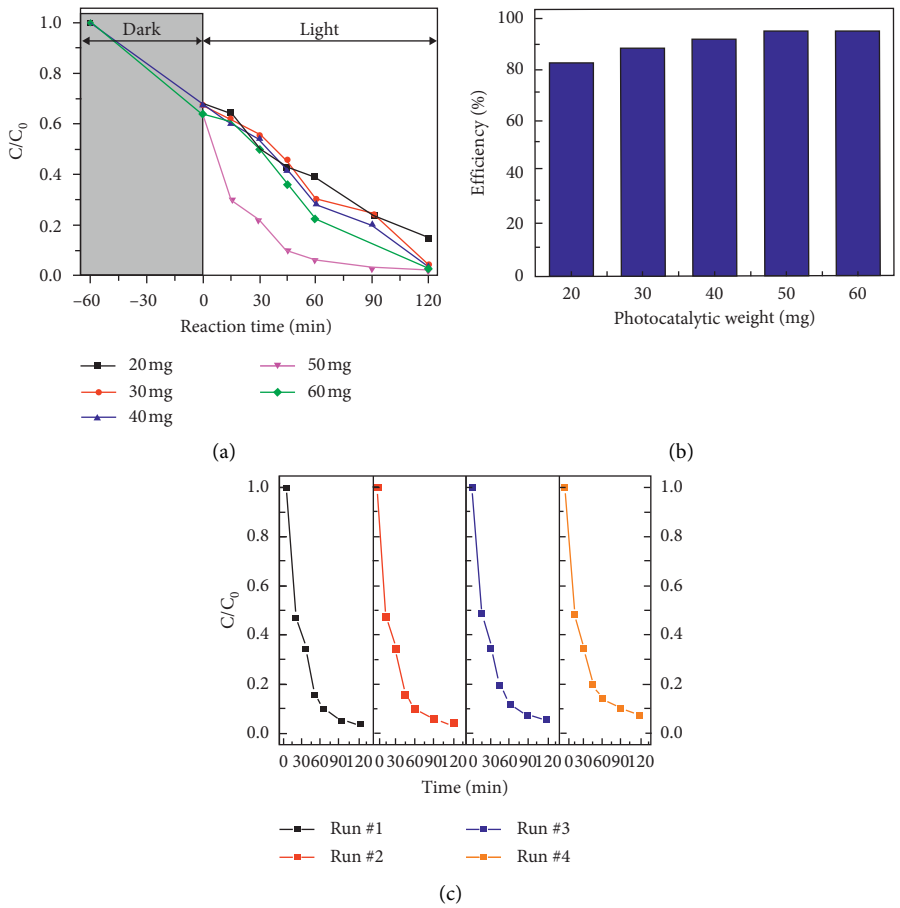

Figure 6: (a) Photocatalytic degradation of MB under visible-light irradiation of Z-7C sample with the different photocatalytic amount. (b) The photocatalytic performance of MB under visible-light irradiation of Z-7C sample on photocatalytic weights. (c) Cyclic performance of the Z-7C photocatalysts towards MB under visible-light irradiation.

Table 2: A comparison of photocatalytic activity of g-C_3N_4@ZnO (7%) on the degradation of MB under visible light with recently reported catalysts.

Catalyst	Dye conc. (ppm)	Catalyst amount (mg)	Solution volume (ml)	Time (min)	Light power (watt)	Degradation (%)	Constant rate k (min^{-1})	References
ZnO/g-C_3N_4	10	—	100	50	500	95	0.038	[41]
ZnO–CN	10	20	100	150	UV light 365 nm	99	0.012	[42]
g-C_3N_4/ZnO	1	20	30	90	Mild UV	99	—	[43]
g-C_3N_4/ AgBr/ZnO	5	40	100	80	300	96.3	0.041	[44]
g-C_3N_4@ZnO	10	50	100	120	250	96.8	0.032	Present study

were similar to the aforementioned photocatalytic activity tests, except for the addition of scavengers to the MB solution before visible-light irradiation. The concentrations of TEOA, IPA, and BQ were 10, 10, and 1 mmol L^{-1}, respectively.

The MB degradation rates with different scavengers were summarized in Figure 8.(b) The results indicate that a large number of $\cdot O_2^-$ were generated when g-C_3N_4@ZnO was irradiated under visible light and played an important role in the degradation of the MB. Therefore, degradation of the dyes was slightly suppressed when isopropyl alcohol was added because of a small amount of OH generated through $\cdot O_2^-$ reacting with H^+. Degradation of the MB was significantly inhibited because of the addition of benzoquinone to capture $\cdot O_2^-$.

The recombination of electrons and holes was restrained when TEOA was added to the system as a scavenger to capture holes. At the same time, more electrons migrated to the surface of the photocatalyst and reacted with O_2 to form $\cdot O_2^-$, which could enhance the degradation of the MB under visible-light irradiation by g-C_3N_4@ZnO. Therefore, the main active species are ·OH, $\cdot O_2^-$, and h^+ in the MB

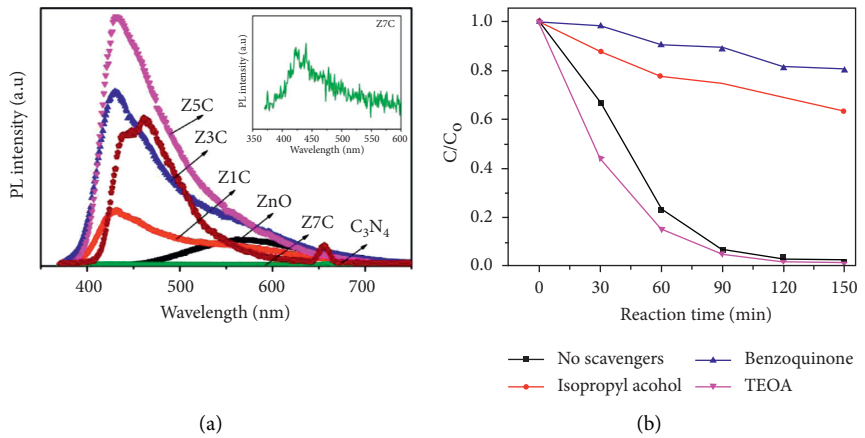

(a) (b)

Figure 7: (a) PL spectra of ZnO, g-C_3N_4, and g-C_3N_4@ZnO composite. (b) Results of active species trapping experiments.

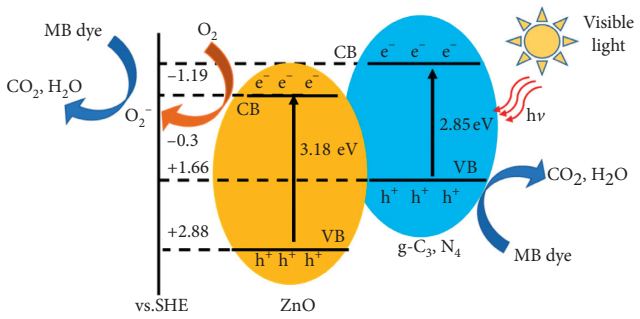

Figure 8: Simplified schematic diagram of the energy band structure and electron-hole pair separation in g-C_3N_4@ZnO nanocomposite.

degradation process. The result is following the reported results [47, 50, 51].

The enhanced photocatalytic activity of g-C_3N_4@ZnO nanocomposite under visible-light irradiation can be explained as follows (Figure 8): The band positions of the g-C_3N_4@ZnO can be calculated by the following empirical formulas [25, 41, 52]:

$$E_{VB} = X + 0.5Eg - Ee, \quad (5)$$

$$E_{CB} = E_{VB} - Eg, \quad (6)$$

where E_{VB} is the valence band potential; E_{CB} is the conduction band potential; X is the absolute electronegativity of the semiconductor; Ee is the energy of free electrons on the hydrogen scale ($Ee = 4.5$ eV). The X values for g-C_3N_4 and ZnO are 4.73 and 5.79 eV, respectively. Eg is the bandgap of the semiconductor and it can be extracted from reflectance spectra data.

According to Equations (5) and (6), the value E_{CB} of g-C_3N_4 and ZnO is about −1.19 and −0.3 eV, respectively. E_{VB} of g-C_3N_4 and ZnO are estimated to be 1.66 and 2.88 eV, respectively. The result is following the reported results [25, 29, 35, 36].

Under visible-light irradiation, only g-C_3N_4 absorbed visible light and was excited. Because the conduction band (CB) edge of g-C_3N_4 was more negative than that of ZnO, the photoinduced electrons on CB of g-C_3N_4 can transfer easily to the CB of ZnO [42], while the holes in the VB of g-C_3N_4 could oxidize MB directly. Moreover, electrons in the CB of ZnO were trapped by O_2 dissolved in the solution to generate superoxide radicals, which could further oxidize the MB.

4. Conclusions

In summary, the in situ heterojunction structure of g-C_3N_4@ZnO nanocomposites with different g-C_3N_4 contents (0, 1, 3, 5, and 7 wt.%) was prepared via a one-step hydrothermal method. The direct introduction of g-C_3N_4 into nanocomposite causes the decrease of crystalline size, optical bandgap, and the change of morphology of nanocomposite. g-C_3N_4 remarkably enhances the photocatalytic performance of g-C_3N_4@ZnO nanocomposites under visible-light irradiation in comparison with pure ZnO. Nanocomposite having 7 wt.% of g-C_3N_4 shows the highest photocatalytic activity and good recyclability. The superior photocatalytic performance of the Z-7C nanocomposite was 0.0320 min^{-1}, which is about 24.6 times higher than that of pure ZnO (0.0013 min^{-1}). This enhancement might be assigned to the wider and stronger absorption of visible light of g-C_3N_4@ZnO nanocomposite-narrower optical bandgap and higher absorbance, which are preferable for enhancing photocatalytic performance. Moreover, the g-C_3N_4 lamellar structure is useful for photoinduced carriers to be rapidly transferred, which is beneficial for the direct transfer of photoinduced carriers in heterojunction. These results imply a simple method to prepare an effective photocatalyst working under visible-light irradiation.

Data Availability

The data are available upon request.

Conflicts of Interest

The authors declare that they have no conflicts of interest.

Acknowledgments

This research was funded by the Hanoi University of Science and Technology (HUST) under Project no. T2018-TĐ-203.

Supplementary Materials

XRD pattern of g-C_3N_4 is shown in Figure S1. The characteristic diffraction peaks of the pure g-C_3N_4 appearing at 27.4° and 13.1° can be indexed to the (002) and (100) planes, which are attributed to the characteristic interlayer structure and interplanar stacking peaks of aromatic systems, respectively. We can evaluate based on the plot of $[F(R) * h\nu]^{1/2}$ versus $h\nu$ as shown in Figure S2 for g-C_3N_4 and g-C_3N_4@ ZnO. The optical bandgap of the pure g-C_3N_4 has an optical bandgap of 2.85 eV, which agrees well with the previous reports [29, 39, 40]. Interestingly, the optical bandgap of composites ranges from 3.05 to 3.09 eV and decreases with the increase of g-C_3N_4 content. In detail, the extracted optical bandgaps of nanocomposites Z-1C, Z-3C, Z-5C, and Z-7C are 3.09 eV, 3.08 eV, 3.07 eV, and 3.05 eV, respectively. (*Supplementary Materials*)

References

[1] N. B. Singh, G. Nagpal, S. Agrawal, and Rachna, "Water purification by using adsorbents: a review," *Environmental Technology & Innovation*, vol. 11, pp. 187–240, 2018.

[2] S.-M. Lam, J.-C. Sin, and A. R. Mohamed, "A review on photocatalytic application of g-C3N4/semiconductor (CNS) nanocomposites towards the erasure of dyeing wastewater," *Materials Science in Semiconductor Processing*, vol. 47, pp. 62–84, 2016.

[3] O. Sacco, D. Sannino, and V. Vaiano, "Packed bed photoreactor for the removal of water pollutants using visible light emitting diodes," *Applied Sciences*, vol. 9, no. 3, pp. 472–486, 2019.

[4] P. Singh, R. Kant, A. Rai, A. Gupta, and S. Bhattacharya, "Facile synthesis of ZnO/GO nanoflowers over Si substrate for improved photocatalytic decolorization of MB dye and industrial wastewater under solar irradiation," *Materials Science in Semiconductor Processing*, vol. 89, pp. 6–17, 2019.

[5] K. Ravichandran, K. Kalpana, R. Uma, E. Sindhuja, and K. S. Seelan, "Cost-effective fabrication of ZnO/g-C3N4 composite film coated stainless steel meshes for visible light responsive photocatalysis," *Materials Research Bulletin*, vol. 99, pp. 268–280, 2018.

[6] M. Balık, V. Bulut, and I. Y. Erdogan, "Optical, structural and phase transition properties of Cu2O, CuO and Cu2O/CuO: Their photoelectrochemical sensor applications," *International Journal of Hydrogen Energy*, vol. 44, no. 34, pp. 18744–18755, 2019.

[7] K. J. Myung, Y. Hyejin, L. Wonjoo, and C. G. Hyun, "Enhancing photoresponse of nanoparticulate α-Fe2O3 electrodes by surface composition tuning," *Journal of Physics and Chemistry of Solids*, vol. 130, pp. 93–99, 2019.

[8] S. Ghoh, R. Vasant Kumar, and M. Coto, *Visible Light Active Photocatalysis: Nanostructured Catalyst Design Mechanisms and Applications*, pp. 447–473, Wiley-VCH Verlag GmbH & Co., Hoboken, NJ, USA, 2018.

[9] S. Bera, D.-I. Won, S. B. Rawal, H. J. Kang, and W. I. Lee, "Design of visible-light photocatalysts by coupling of inorganic semiconductors," *Catalysis Today*, vol. 335, pp. 3–19, 2019.

[10] S. Ghosh, C. Raviola, and S. Protti, "Visible-solar-light-driven photocatalytic degradation of phenol with dye-sensitized TiO2: parametric and kinetic study," *Industrial & Engineering Chemistry Research*, vol. 2, no. 2, pp. 27–51, 2018.

[11] Z. Sabouri, A. Akbari, H. A. Hosseini, and M. Darroudi, "Facile green synthesis of NiO nanoparticles and investigation of dye degradation and cytotoxicity effects," *Journal of Molecular Structure*, vol. 1173, pp. 931–936, 2018.

[12] L. Valenzuela, A. Iglesias, M. Faraldos, A. Bahamonde, and R. Rosal, "Antimicrobial surfaces with self-cleaning properties functionalized by photocatalytic ZnO electrosprayed coatings," *Journal of Hazardous Materials*, vol. 369, pp. 665–673, 2019.

[13] K. H. Le, O. L. K. Pham, T. T. Tran, and V. M. Le, "Photocatalytic activities of sulfur doped SrTiO3 under simulated solar irradiation," *Science and Technology Development Journal*, vol. 19, no. 3, pp. 176–184, 2016.

[14] Q. Pengpeng, P. Beomguk, C. Jongbok, T. Binota, P. B. Aniruddha, and K. Jeehyeong, "Understanding TiO_2 Photocatalysis: Mechanisms and Materials," *Ultrasonic Sonochemistry*, vol. 45, pp. 29–49, 2018.

[15] K. Qi, B. Cheng, J. Yu, and W. Ho, "Review on the improvement of the photocatalytic and antibacterial activities of ZnO," *Journal of Alloys and Compounds*, vol. 727, pp. 792–820, 2017.

[16] V. L. Reddy Pullagurala, I. O. Adisa, S. Rawat et al., "Finding the conditions for the beneficial use of ZnO nanoparticles towards plants-A review," *Environmental Pollution*, vol. 241, pp. 1175–1181, 2018.

[17] S. Kumar, A. Dhiman, P. Sudhagar, and V. Krishnan, "ZnO-graphene quantum dots heterojunctions for natural sunlight-driven photocatalytic environmental remediation," *Applied Surface Science*, vol. 447, pp. 802–815, 2018.

[18] M. Azarang, A. Shuhaimi, R. Yousefi, A. Moradi Golsheikh, and M. Sookhakian, "Synthesis and characterization of ZnO NPs/reduced graphene oxide nanocomposite prepared in gelatin medium as highly efficient photo-degradation of MB," *Ceramics International*, vol. 40, no. 7, pp. 10217–10221, 2014.

[19] F. Hosseini, A. Kasaeian, F. Pourfayaz, M. Sheikhpour, and D. Wen, "Novel ZnO-Ag/MWCNT nanocomposite for the photocatalytic degradation of phenol," *Materials Science in Semiconductor Processing*, vol. 83, pp. 175–185, 2018.

[20] J. Longbo, Y. Xingzhong, P. Yang et al., "Tuning the morphology of g-c3n4 for improvement of z-scheme photocatalytic water oxidation," *Applied Catalysis B: Environmental*, vol. 217, pp. 388–406, 2017.

[21] E. Chubenko, I. Gerasimenko, V. Bondarenko, and D. Zhigulin, "Zinc oxide nanostructures doped with transition metals: fabrication and properties," *International Journal of Nanoscience*, vol. 18, pp. 1–4, 2019.

[22] R. Taziwa, L. Ntozakhe, and M. Edson, "Novel green-chemistry micro-fluidic synthesis of anthracene-based microporous for H_2 storage by capillary-furnace LED based reactor," *Journal of Nanoscience and Nanotechnology*, vol. 1, no. 13, pp. 1–8, 2017.

[23] X. Wan, W. Ma, J. Yang et al., "A comprehensive review on emerging artificial neuromorphic devices," *The Journal of Alloys and Compounds*, vol. 737, pp. 197–206, 2018.

[24] Z. Youssef, L. Colombeau, N. Yesmurzayeva et al., "Dye-sensitized nanoparticles for heterogeneous photocatalysis: cases studies with TiO_2, ZnO, fullerene and graphene for

water purification," *Dyes and Pigments*, vol. 159, pp. 49–71, 2018.

[25] L. Lu, Z. Lv, Y. Si, M. Liu, and S. Zhang, "Recent progress on band and surface engineering of graphitic carbon nitride for artificial photosynthesis," *Applied Surface Science*, vol. 462, pp. 693–712, 2018.

[26] L. Jiang, X. Yuan, Y. Pan et al., "Doping of graphitic carbon nitride for photocatalysis: a reveiw," *Applied Catalysis B: Environmental*, vol. 217, pp. 388–406, 2017.

[27] D. Masih, Y. Ma, and S. Rohani, "Graphitic C3N4 based noble-metal-free photocatalyst systems: a review," *Applied Catalysis B: Environmental*, vol. 206, pp. 556–588, 2017.

[28] I. Michio, T. Tomoki, K. Tarou, and T. Masahiro, "Graphitic carbon nitrides (g-C3N4) with comparative discussion to carbon materials," *Carbon*, vol. 141, pp. 580–607, 2019.

[29] I. M. Sundaram, S. Kalimuthu, and G. Ponniah, "Highly active ZnO modified g-C 3 N 4 Nanocomposite for dye degradation under UV and Visible Light with enhanced stability and antimicrobial activity," *Composites Communications*, vol. 5, pp. 64–71, 2017.

[30] W.-K. Jo and N. Clament Sagaya Selvam, "Enhanced visible light-driven photocatalytic performance of ZnO-g-C3N4 coupled with graphene oxide as a novel ternary nanocomposite," *Journal of Hazardous Materials*, vol. 299, pp. 462–470, 2015.

[31] G. Mamba and A. K. Mishra, "Graphitic carbon nitride (g-C 3 N 4) nanocomposites: a new and exciting generation of visible light driven photocatalysts for environmental pollution remediation," *Applied Catalysis B: Environmental*, vol. 198, pp. 347–377, 2016.

[32] P. Praus, L. Svoboda, M. Ritz, I. Troppová, M. Šihor, and K. Kočí, "Graphitic carbon nitride: synthesis, characterization and photocatalytic decomposition of nitrous oxide," *Materials Chemistry and Physics*, vol. 193, pp. 438–446, 2017.

[33] M. A. Ismail, K. K. Taha, A. Modwi, and L. Khezami, "ZnO nanoparticles: surface and X-ray profile analysis," *Journal of Ovonic Research*, vol. 14, no. 5, pp. 381–393, 2018.

[34] V. Mote, Y. Purushotham, and B. Dole, "Williamson-Hall analysis in estimation of lattice strain in nanometer-sized ZnO particles," *Journal of Theoretical and Applied Physics*, vol. 6, no. 1, pp. 2–9, 2012.

[35] N. C. Tu, P. V. Thang, L. T. Lan Anh et al., "Size and crystallinity-dependent magnetic properties of CoFe2O4 nanocrystals," *Ceramics International*, vol. 46, no. 7, pp. 8711–8718, 2020.

[36] R. López and R. Gómez, "Band-gap energy estimation from diffuse reflectance measurements on sol-gel and commercial TiO2: a comparative study," *Journal of Sol-Gel Science and Technology*, vol. 61, no. 1, pp. 1–7, 2012.

[37] A. Sáenz-Trevizo, P. Amézaga-Madrid, P. Pizá-Ruiz, W. Antúnez-Flores, and M. Miki-Yoshida, "Optical band gap estimation of ZnO nanorods," *Materials Research*, vol. 19, no. 1, pp. 33–38, 2016.

[38] E. L. Simmons, "Reflectance spectroscopy: application of the Kubelka-Munk theory to the rates of photoprocesses of powders," *Applied Optics*, vol. 15, no. 4, pp. 951–954, 1976.

[39] W. Liu, M. Wang, C. Xu, and S. Chen, "Facile synthesis of g-C3N4/ZnO composite with enhanced visible light photooxidation and photoreduction properties," *Chemical Engineering Journal*, vol. 209, pp. 386–393, 2012.

[40] L. Wang, C. Ma, Z. Guo et al., "In-situ growth of g-C3N4 layer on ZnO nanoparticles with enhanced photocatalytic performances under visible light irradiation," *Materials Letters*, vol. 188, pp. 347–350, 2017.

[41] S. Prabhu, M. Pudukudy, S. Harish et al., "Facile construction of djembe-like ZnO and its composite with g-C3N4 as a visible-light-driven heterojunction photocatalyst for the degradation of organic dyes," *Materials Science in Semiconductor Processing*, vol. 106, Article ID 104754, 2020.

[42] A. Mohammad, K. Ahmad, A. Qureshi, M. Tauqeer, and S. M. Mobin, "Zinc oxide-graphitic carbon nitride nanohybrid as an efficient electrochemical sensor and photocatalyst," *Sensors and Actuators B: Chemical*, vol. 277, pp. 467–476, 2018.

[43] S. P. Adhikari, H. R. Pant, H. J. Kim, C. H. Park, and C. S. Kim, "A highly sensitive, selective and room temperature operatable formaldehyde gas sensor using chemiresistive g-C3N4/ZnO," *Ceramics International*, vol. 41, pp. 12923–12929, 2015.

[44] E. Boorboor Azimi, A. Badiei, and M. Hossaini Sadr, "Dramatic visible photocatalytic performance of g-C3N4-based nanocomposite due to the synergistic effect of AgBr and ZnO semiconductors," *Journal of Physics and Chemistry of Solids*, vol. 122, pp. 174–183, 2018.

[45] W. Liu, M. Wang, C. Xu, S. Chen, and X. Fu, "Significantly enhanced visible-light photocatalytic activity of g-C3N4 via ZnO modification and the mechanism study," *Journal of Molecular Catalysis A: Chemical*, vol. 368–369, no. 369, pp. 9–15, 2013.

[46] D. Ren, "A terpolymer acceptor enabling all-polymer solar cells with a broad donor:acceptor composition tolerance and enhanced stability," *Solar RRL*, vol. 4, no. 8, pp. 1–11, 2020.

[47] B. Chai, J. Yan, G. Fan, G. Song, and C. Wang, "In situ fabrication of CdMoO4/g-C3N4 composites with improved charge separation and photocatalytic activity under visible light irradiation," *Chinese Journal of Catalysis*, vol. 41, no. 1, pp. 170–179, 2020.

[48] J. Liu, "A review of multi-physical fields induced phenomena and effects in spark plasma sintering: fundamentals and applications," *Journal of Materials Science*, vol. 46, no. 4, pp. 888–892, 2017.

[49] L. T. L. Anh, M. M. Neto, P. V. Thang, N. T. T. Mai, N. X. Sang, and N. C. Tu, "Optical and photocatalytic properties of in-situ gr@ZnO microspindle composites prepared by hydrothermal method," *Journal of Nanoscience and Nanotechnology*, vol. 21, no. 4, pp. 2653–2659, 2021.

[50] L. Hu, J. Yan, C. Wang, B. Chai, and J. Li, "Direct electrospinning method for the construction of Z-scheme TiO2/g-C3N4/RGO ternary heterojunction photocatalysts with remarkably ameliorated photocatalytic performance," *Chinese Journal of Catalysis*, vol. 40, no. 3, pp. 458–469, 2019.

[51] A. I. Navarro-Aguilar, S. Obregón, D. Sanchez-Martinez, and D. B. Hernández-Uresti, "An efficient and stable WO3/g-C3N4 photocatalyst for ciprofloxacin and orange G degradation," *Journal of Photochemistry and Photobiology A: Chemistry*, vol. 384, Article ID 112010, 2019.

[52] M. Karimi-Nazarabad and E. K. Goharshadi, "Photocatalytic mineralization of hard-degradable morphine by visible light-driven Ag@g-C3N4 nanostructures," *Solar Energy Materials and Solar Cells*, vol. 160, pp. 484–493, 2017.